Heliyon 10 (2024) e23688

Contents lists available at ScienceDirect

Heliyon

journal homepage: www.cell.com/heliyon

Brachyolmia, dental anomalies and short stature (DASS): Phenotype and genotype analyses of Egyptian and Pakistani patients

Hamed Nawaz [a,1], Asia Parveen [b,n,1], Sher Alam Khan [a,c], Abul Khair Zalan [d], Muhammad Adnan Khan [e], Noor Muhammad [a], Nehal F. Hassib [f,g], Mostafa I. Mostafa [f], Rasha M. Elhossini [h], Nehal Nabil Roshdy [i], Asmat Ullah [j,k], Amina Arif [n], Saadullah Khan [a,**], Ole Ammerpohl [l], Naveed Wasif [l,m,*]

[a] *Department of Biotechnology and Genetic Engineering, Kohat University of Science and Technology (KUST), Kohat, Pakistan*
[b] *Department of Biochemistry, Faculty of Life Sciences, Gulab Devi Educational Complex, Gulab Devi Hospital, 54000, Lahore, Pakistan*
[c] *Department of Computer Science and Bioinformatics, Khushal Khan Khatak University, Karak, Pakistan*
[d] *BDS, MDS Registrar Pediatric Dentistry, Department of Pediatric Dentistry, School of Dentistry, PIMS, Islamabad, Pakistan*
[e] *Dental Material, Institute of Basic Medical Sciences, Khyber Medical University Peshawar, Peshawar, Pakistan*
[f] *Orodental Genetics Department, Human Genetics and Genome Research Institute, National Research Centre, Cairo, 12622, Egypt*
[g] *School of Dentistry, New Giza University, Giza, Egypt*
[h] *Clinical Genetics Department, Human Genetics and Genome Research Institute, National Research Centre, Cairo, 12622, Egypt*
[i] *Endodontics, Faculty of Dentistry, Cairo University, Cairo, 11553, Egypt*
[j] *Department of Biomedicine, Aarhus University, Aarhus, Denmark*
[k] *The Novo Nordisk Foundation Center for Genomic Mechanisms of Disease, Broad Institute of MIT and Harvard, Cambridge, MA, 02142, USA*
[l] *Institute of Human Genetics, Ulm University and Ulm University Medical Center, 89081, Ulm, Germany*
[m] *Institute of Human Genetics, University Hospital Schleswig-Holstein, Campus Kiel, D-24105, Kiel, Germany*
[n] *Faculty of Science and Technology, University of Central Punjab (UCP), Lahore, Pakistan*

ARTICLE INFO

Keywords:
Amelogenesis imperfecta
Brachyolmia
Exome sequencing
Frameshift variants
Hearing impairment
Homozygous splice acceptor site
LTBP3

ABSTRACT

Brachyolmia is a heterogeneous group of developmental disorders characterized by a short trunk, short stature, scoliosis, and generalized platyspondyly without significant deformities in the long bones. DASS (Dental Abnormalities and Short Stature), caused by alterations in the *LTBP3* gene, was previously considered as a subtype of brachyolmia.

The present study investigated three unrelated consanguineous families (A, B, C) with Brachyolmia and DASS from Egypt and Pakistan. In our Egyptian patients, we also observed hearing impairment. Exome sequencing was performed to determine the genetic causes of the diverse clinical conditions in the patients. Exome sequencing identified a novel homozygous splice acceptor site variant (*LTBP3*:c.3629-1G > T; p. ?) responsible for DASS phenotypes and a known homozygous missense variant (*CABP2*: c.590T > C; p.Ile197Thr) causing hearing impairment in the Egyptian patients. In addition, two previously reported homozygous frameshift variants (*LTBP3*:c.132delG; p.Pro45Argfs*25) and (*LTBP3*:c.2216delG; p.Gly739Alafs*7) were identified in Pakistani patients.

* Corresponding author. Institute of Human Genetics, University Hospital Schleswig-Holstein, Campus Kiel, D-24105, Kiel, Germany
** Corresponding author.
E-mail addresses: saad@kust.edu.pk (S. Khan), naveedwasif@gmail.com (N. Wasif).
[1] The authors have equally contributed to this work.

https://doi.org/10.1016/j.heliyon.2023.e23688
Received 14 April 2023; Received in revised form 29 November 2023; Accepted 9 December 2023
Available online 14 December 2023

This study emphasizes the vital role of *LTBP3* in the axial skeleton and tooth morphogenesis and expands the mutational spectrum of *LTBP3*. We are reporting *LTBP3* variants in seven patients of three families, majorly causing brachyolmia with dental and cardiac anomalies. Skeletal assessment documented short webbed neck, broad chest, evidences of mild long bones involvement, short distal phalanges, pes planus and osteopenic bone texture as additional associated findings expanding the clinical phenotype of DASS. The current study reveals that the hearing impairment phenotype in Egyptian patients of family A has a separate transmission mechanism independent of *LTBP3*.

1. Introduction

Brachyolmia is a rare heterogeneous group of axial skeletal dysplasias, characterized clinically by short trunk, mild short stature, scoliosis, as well as generalized platyspondyly (flattened vertebral bodies), rectangular shaped vertebrae with short pedicles and posterior scalloping, narrow intervertebral spaces and narrow interpedicular distances shown radiographically. In most cases, Brachyolmia is associated with almost no significant anomalies (metaphyseal, epiphyseal, or diaphyseal) in long bones [1]. Axial skeletal disorder usually appears during childhood; however, short stature becomes more evident later in life [2].

Based on the clinical and radiological features of the patients and the inheritance patterns of the disease, Brachyolmia can be classified into various types, including Brachyolmia type-1/Toledo/Hobaek type (OMIM: 271630, 271530; *PAPSS2*: OMIM: 603005; 10q23.2-q23.31), Brachyolmia type-2/Maroteaux type (OMIM: 613678; *PAPSS2*: OMIM: 603005; 10q23.2-q23.31), Brachyolmia type-3 (OMIM: 113500; *TRPV4*: OMIM: 605427; 12q24.11), Brachyolmia type-4 (OMIM: 612847; *PAPSS2*: OMIM: 603005; 10q23.2-q23.31), and Brachyolmia type-5, associated with short stature and dental anomalies in the form of amelogenesis imperfecta/hypodontia (DASS; OMIM: 601216) that is caused by pathogenic homozygous variants in Latent TGF-beta binding protein 3 (*LTBP3*) (OMIM: 602090; 11q13.1) [3].

The pathogenicity profile of *LTBP3* is broad and is involved in causing several disease conditions, including DASS and thoracic aortic aneurysm [4], acromicric dysplasia (ACMICD), and geleophysic dysplasia 3 (GPHYSD3, OMIM: 617809) [5]. Recently, Kantaputra et al., 2022 [6] reported heterozygous compound variants in a Turkish family, where heterozygous carriers showed mild phenotypes for the first time compared to the affected female patient carrying both heterozygous variants. According to the Human Gene Mutation Database (HGMD Professional 2022.1), a total of thirty-four variants have been identified in *LTBP3*; out of these, only 11 variants are causing DASS [3–10] (Suppl. Table 1).

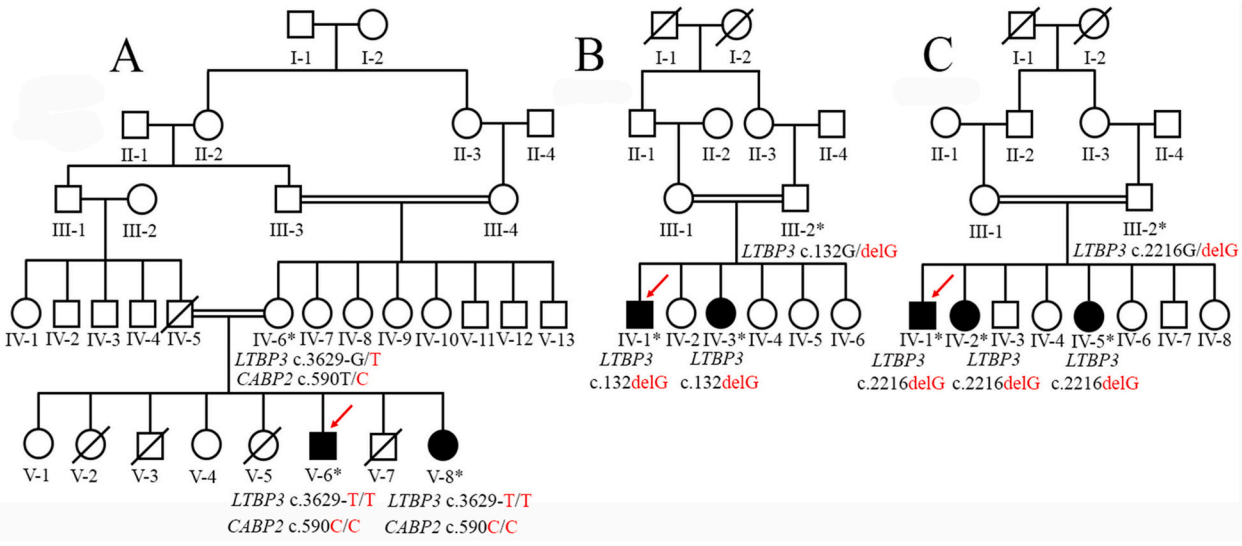

Fig. 1. (A) Pedigree of family A (B) Pedigree of family B (C) Pedigree of family C. Empty squares and circles represent unaffected male and female individuals respectively. The crossed shapes represent the deceased individuals. Affected male and female participants are represented by filled squares and circles respectively. The symbols labelled with asterisks represent the individuals who participated in this study. The arrows (red) show the probands, who were subjected to exome sequencing. All pedigrees show autosomal recessive inheritance. The genotypes are written below the symbol of each participating member. In case of *LTBP3* variant in family A the mother (IV-6) is heterozygous (G/T), while both the affected siblings (V-6 and V-8) are homozygous (T/T) for the splice site variant c.3629-1G > T, in case of *CABP2* the mother (IV-6) is heterozygous (T/C), while both the patients (V-6 and V-8) are homozygous (C/C) for the missense variant c.590T > C. In family B, the father (III-2) is heterozygous (G/-), while both the affected siblings (IV-1 and IV-3) are homozygous (−/−) for the variant c.132delG; p.Pro45Argfs*25. In family C, the father (III-2) is heterozygous (G/-), while all the affected members are homozygous for the variant c.2216delG; p.Gly739Alafs*7.

LTBP3 is an essential extracellular matrix (ECM) multi-domain component. It is necessary for the bioavailability of transforming growth factor beta (TGF-β) by regulating its secretion, folding, activation, and deposition into the ECM of chondrocytes [11]. LTBP3 is highly expressed in developing teeth and bones, the cardiac outflow tract, and the walls of major blood vessels [9].

CABP2 (OMIN: 607314) is mapped on chromosome 11q13.3 [12], consisting of seven exons, and encoding 220 amino acids lengthy calcium-binding protein 2 (CABP2). CABP2 is highly expressed in the cochlea and is involved in modulation of the presynaptic influx of Ca^{2+} in the inner hair cells, affecting the further transmission of auditory messages to the brain through voltage Ca^{2+} channels in a Ca^{2+} dependent manner [13]. CABP2 is a vital regulator of hearing sensitivity in inner hair cells and is mandatory for the peripheral auditory system's normal function [14].

The current study aims to investigate the phenotypes and genotypes of three unrelated consanguineous families with seven affected individuals from Egypt and Pakistan. The patients showed DASS (dental abnormalities including amelogenesis imperfecta, tooth agenesis, and short stature) phenotypes. Moreover, Egyptian patients had associated hearing loss. In the previous studies, no detailed LTBP3-associated disease phenotype comparison study was undertaken, which is why the present study intends to compare the phenotypes of our patients with previously reported patients according to the mutation types, their location in the gene, and loss of LTBP3 functional domains. This study strengthens and supports the pivotal role of the *LTBP3* gene in the development of heart, teeth, and skeletal structures. The phenotypic and mutational expansions encourage the phenotype-genotype correlation.

2. Materials and methods

2.1. Study approval, families' recruitment, blood collection, and genomic DNA (gDNA) extraction

The Oro-dental Genetics Reviewer scientific board of the department, National Research Centre (NRC), and the Local project (12060202) approved by the Ethical Committee of the National Research Centre, Cairo, Egypt, and Research and Ethical Committee (certificate no. 1998), of Kohat University of Science and Technology, Kohat, Pakistan, approved the study. These committees followed the recommendations of the Declarations of Helsinki.

Regarding pedigrees, the three pedigrees showed autosomal recessive inheritance patterns with positive parental consanguinity. Family A showed a five-generation pedigree, in which two affected siblings (V-6 and V-8) and their mother (IV-6) participated in this study (Fig. 1A). Family B showed a four-generation pedigree having two affected individuals (IV-1 and IV-3), and their father (III-2) participated in the study (Fig. 1B). Finally, Family C consisted of four generation pedigree; three affected individuals (IV-1, IV-2, and IV-5) and their father (III-2) participated in this study (Fig. 1C). Informed and written consent was taken from all the participants. Genomic DNA (gDNA) was isolated from the whole peripheral blood of the participants using the Promega gDNA extraction kit (Madison, Wisconsin, USA).

2.2. Exome sequencing in family A

A 100 ng/μl gDNA of two members (IV-1 and IV-4) was used for exome sequencing. After preparing the sequencing libraries using the SeqCap EZ human exome library v2.0 kit, the Illumina HiSeq 4000 sequencing machine via a paired-end 100-bp protocol (Hussain et al., 2013) was used for sequencing. Illumina real-time analysis (RTA) software v1.8 was used to filter the primary data, followed by the human reference genome build GRCh37/hg19 (http://www.genome.ucsc.edu/) for mapping the reads, using the BWA-SW alignment algorithm. Picard tools and the Genome Analysis Toolkit (GATK) were used to improve the reads quality for realignment and base quality score recalibration. The Platypus, Haplotype Caller, and Mpileup programs were used to perform the calling of single nucleotide polymorphisms (SNPs) and short insertions/deletions (INDELs). The variant quality score calibration (VQSR) using GATK was used for further filtration. The ALLEGRO program identified the large runs of homozygosity (ROH) based on multipoint linkage analysis. The CNMOPS and ExomeDepth algorithms were utilized to check the coverage of CNVs, and the variants data was combined and annotated using the COMBINE and FUNC algorithms.

2.3. Variant identification and classification

The exome data analysis was performed using the Varbank pipeline v2.26 (https://varbank.ccg.uni-koeln.de/) of Cologne Center for Genomics (CCG), Cologne, Germany. The mean coverage of the data was 93 %, while at 20X and 10X, the coverage of the targeted bases was 96.3 and 98.8 %, respectively. The ROH in the affected members ($\geq$5 Mb) were identified, considering the autosomal recessive pedigree. The rare homozygous variants lying in these ROH were considered for further analysis. The allele read frequency (75%–100 %) for homozygous changes and allele frequency (<1 %) for recessive variants were used during filtration. The VarSome [15], Human Gene Mutation Database (HGMD) Professional 2022.1, and Database of Single Nucleotide Polymorphisms (dbSNP) were utilized for evaluation of the variants. In addition, Genome Aggregation Database v.2.1.1 (gnomAD; https://gnomad.broadinstitute.org/) was consulted to establish the minor allele frequency (MAF; value < 0.01) of the variants. An in-house database of 650 exomes of patients with diverse phenotypes of various ethnic backgrounds, including ten exomes of Egyptian and 100 exomes of Pakistani ethnic group, were employed as a control. ACMG guidelines were consulted to classify pathogenic, likely pathogenic, likely benign, uncertain significance, and benign variants [16].

After performing the exome data analysis, all the gene variants were filtered and validated in various databases, including Single Nucleotide Polymorphism Database (dbSNP, https://www.ncbi.nlm.nih.gov/snp/), 1000 genome project (https://www.internationalgenome.org/), Exome Variant Server Database (EVS, https://evs.gs.washington.edu/EVS/), and gnomAD (https://

gnomad.broadinstitute.org/). The reference sequences were obtained from the University of California Santa Cruz (UCSC) genome database browser (http://genome.ucsc.edu/cgi-bin/hgGateway).

2.4. Exome sequencing in families B and C

A 100 μg/μl gDNA of the affected individuals IV-1 and IV-1 in families B and –C respectively, was used for hybridization-based exome enrichment. xGen Exome Research Panel v2 (Integrated DNA Technologies, Coralville, Iowa, USA) was used to capture the exonic regions of ~22,000 human genes. Thereafter, Novaseq 6000 (Illumina, San Diego, CA, USA) was used for sequencing the captured regions of the genome. In case of family B, sequencing generated high-quality reads, i.e., 99.4 bases covered $\geq$ 1X, 99.2 $\geq$ 5X, 99.1 $\geq$ 10X, 99.0 $\geq$ 20X, and 97.0 $\geq$ 50X with a mean target coverage depth of 150.3X. Alignment to the GRCh37/hg19 human reference genome, variant calling, and annotation was conducted with open-source bioinformatics tools, including BWA-MEM (v.0.7.17) [17], Samtools (v.1.9) [18], Picard (v.2.20.8) (http://broadinstitute.github.io/picard/) and HaplotypeCaller of GATK (v.3.8) [19] and in-house software. However, in case of family-C, a total of 9,651,984,405 bases of the sequence were generated and aligned to the Genome Reference Consortium Human Build 37 (GRCh37) and Revised Cambridge Reference Sequence (rCRS) of the mitochondrial genome, generating 136.45 mean depth-of-coverage within the 34,366,188 bases of the captured region, which is approximately 99.3 % of the Reference Sequence (RefSeq) protein-coding region. Approximately 99.00 % of the targeted bases were covered to a depth of $\geq$20×. In total, 66,275 single nucleotide variants (SNV) and 10,976 small insertions and deletions (indel) were identified. Despite the insufficient coverage across 1.00 % of the bases, these metrics were consistent with high-quality exome sequencing data and deemed adequate for analysis.

2.5. Variant identification, and classification

In both families (B, C), variant interpretation was performed, using automatic variant interpretation software EVIDENCE [20], which was developed in-house to prioritize variants based on the guidelines recommended by the American College of Medical Genetics and Genomics (ACMG) and the Association for Molecular Pathology (AMP) [16] in the context of the patients' phenotypes and relevant family history. gnomAD (http://gnomad.broadinstitute.org/) and the 3 billion genome databases were used for estimating the allele frequency. Common variants with a minor allele frequency of (<1 %) were filtered out under BA1 of the ACMG guideline [16]. Evidence data on the pathogenicity of variants were extracted from scientific literature and disease databases, including, ClinVar (https://www.ncbi.nlm.nih.gov/clinvar/) and UniProt (https://www.uniprot.org/). Only variants deemed clinically significant and relevant to the patients' primary clinical indications at the time of variant interpretation were considered. Different databases, including OMIM (Online Mendelian Inheritance in Man) (https://www.omim.org/), gnomAD (genome Aggregation Database), ClinVar (https://ncbi.nlm.nih.gov/clinvar), HGVS (Human Genome Variation Society) (https://www.hgvs.org/) and HGMD (The Human Gene Mutation Database) (http://www.hgmd.cf.ac.uk/ac/index.php) were used during the variant interpretation. The pathogenicity of the variant on its associated disease was evaluated according to the recommendations of ACMG guidelines. The patient's clinical phenotypes were transformed to corresponding standardized human phenotype ontology terms (https://hpo.jax.org/) and accessed to measure the similarity [21,22] with each of ~7000 rare genetic diseases (https://omim.org/and https://www.orpha.net/consor/cgi-bin/index.php). Afterwards, the association of the candidate gene variants with the disease was evaluated by medical geneticists and doctors of the 3billion company, Seoul, Seoul-t'ukpyolsi, South Korea (https://3billion.io/). Finally, the extracted rare variant was confirmed and validated by Sanger sequencing.

2.6. Sanger sequencing

The identified variants were confirmed and validated by Sanger sequencing in the all three families, using ABI 3500 Genetic Analyzer (Applied Biosystems, Foster City, CA, USA) and the ABI BigDye Terminator Sequencing Kit, V.3.1 (Applied Biosystems). Primers are available upon request to the authors. The four variants were described based on the principles of the Human Genome Variations Society (HGVS) [23]. Nucleotide numbers were derived from GRCh37/hg19 assembly using cDNA sequence of *LTBP3* (NM_001130144.2 (c.3629-1G > T; p. ?), *CABP2* (NM_016366.3; c.590T > C; p.Ile197Thr), *LTBP3*: NM_001130144.3 (c.132del; p. Pro45Argfs*25, c.2216del; p.Gly739Alafs*7).

2.7. Pathogenicity prediction

For *in silico* analysis of the variants, different desktop and online pathogenicity prediction tools were used, including MutationTaster (http://www.mutationtaster.org/), CADD (https://cadd.gs.washington.edu/snv), PolyPhen-2 (http://genetics.bwh.harvard.edu/pph2/), varSEAK (https://varseak.bio/), VarSome (https://varsome.com/), PROVEAN (http://provean.jcvi.org/seq_submit.php), MutPred2 (http://mutpred.mutdb.org/), SIFT (https://sift.bii.a-star.edu.sg/), and FATHMM (http://fathmm.biocompute.org.uk/inherited.html).

3. Results

3.1. Clinical and radiological findings

3.1.1. Family A

An Egyptian 25-year-old male (V-6) and 18-year-old female (V-8) presented with progressive childhood onset short stature. The anthropometric measurements revealed that they were of average weights and head circumferences. Presenting standing and sitting heights were (cm) 146 ± 1, (cm) 137.5 ± 1, and (cm) 72 ± 1, (cm) 65.5 ± 1 upper to lower segment respectively. The two siblings had standard upper to lower segment ratios with greater arm spans than their heights (Table 1).

Clinical examination exhibited that both patients had normal psychomotor development with unaffected mental health. The male patient was observed with a short neck and a broad chest, whereas the female was presented with hypertelorism, short philtrum, and a short webbed neck. Both patients had spinal deformities involving thoracic scoliosis, 5th fingers clinodactyly and pes planus.

Regarding the radiological investigations, spine X-ray showed loss of normal spine curvature, particularly at the cervical levels. The ribs were dysplastic and splayed out. There was a reduction of disc space at all levels. Furthermore, flat and biconcave rectangular vertebrae were observed with broader vertebral bodies than pedicles, typically consistent with brachyolmia. Spinal stenosis could be suspected based on smaller disc spaces and flattened vertebrae (Fig. 2A a, b). Hip X-rays showed bilateral narrow joint spaces in both hips.

Moreover, there were subchondral cysts and calcification at the head of the femur and acetabulum. Also, mild irregularities of the epiphyseal ossification of long bones (femurs) were seen with increased femoral neck/shaft angles than the normal range's upper limits (Fig. 2A c). In addition, anterolateral bowing of the tibia with widened cortices of both the tibia and fibula can be appreciated. No noticeable joint changes were observed in the carpus or other hand bones (Fig. 2A d); however, distal phalanges were shortened in all fingers with normal joints (Fig. 2A e).

In both patients, oral examination was manifested with complete loss of enamel layer and yellow-brown discoloration of the existing dentitions. Remarkable attrition of the permanent teeth was noticed. Increasingly, hypodontia was displayed as well. According to the universal dental numbering system, the female had tooth agenesis in #31 and #41, while the male showed hypodontia in #34. There was generalized spacing in the mid-posterior region of the jaws (Fig. 2A f). Panoramic radiographs showed several root canal treatments in the incisors and premolars of both arches, due to early pulp exposure. In addition, the lamina dura was widening, especially in all anterior teeth. The bone height around the teeth was standard, indicating no alveolar bone loss except in the upper posterior area (Fig. 2A g, h). All abnormal intra-oral findings were consistent with amelogenesis imperfecta (AI), as seen in patients with inherited AI disorders.

Based on the echocardiogram, both patients were unaffected. Eye examination exhibited no ocular abnormalities. Further physiological investigation showed bilateral hearing impairment in both affected members (V-6 and V-8). The male patient (V-6) presented moderate to severe hearing loss (Fig. 3 a, b), while the female patient was characterized in the mild to severe hearing impairment category (Fig. 3 c, d). The speech of both was unaffected.

3.1.2. Family B

Two affected Pakistani siblings, IV-1 and IV-3 (a 13-years old male and 8-year-old female), presented with back pain, dental anomalies, and short stature. On physical examination, they showed a short trunk and mild short stature with short limbs, hands, and feet (brachydactyly). Anthropometric measurements showed that the standing heights of the male (IV-1) and the female (IV-3) patients were (cm) 126 ± 1 and (cm) 112 ± 1, while their sitting heights (upper segment) were recorded as (cm) 57.2 ± 1 and (cm) 56 ± 1, respectively. Their upper- and lower-segment ratios were calculated as 0.8 and 1.0, and their arm spans of 127 cm and 112 cm were observed, respectively. Their occipitofrontal circumferences (OFC) were 51 and 53 cm in the male and female siblings, respectively.

They showed facial dysmorphic features with oval-faced shapes, broad and wider foreheads, thin almond and monolid eyes, bulbous noses, pointed chins, and attached earlobes (Fig. 2B a, b).

The skeletal assessment showed brachyolmia. Spinal stenosis could be suspected based on smaller disc space and flattened vertebrae. The spine curvature disorders, including lordosis, kyphosis, and scoliosis, were not observed. Lower limbs X-ray revealed protrusion of both hips with bilateral narrow joint space and lateral deviation of the patella, especially on the right knee. Moreover, mild deformity of tibia was also observed. No significant joint changes were observed in the carpus or other hand bones except of shortening of the distal phalanges in all fingers. Overall, bones were severely osteopenic as the cortices of almost all the bones were thin (Fig. 2B c, d, e, f).

A transthoracic echocardiogram of the male patient was normal. Although, on Doppler assessment, interatrial/atrial septal aneurysm (ASA) was found with dilation of ascending aorta in patient IV-1 (Fig. 2B g), whereas the female sibling (IV-3) had Secundum atrial septal defect (ASD) with interventricular septum IVS paradox. Moreover, both siblings had atrioventricular (AV) concordance with ventriculoarterial (VA) concordance (Fig. 2B h).

The intra-oral evaluation of both siblings showed the classical phenotypes of the disorder presented with hypodontia and amelogenesis imperfecta. The present teeth had yellow discoloration with reduced enamel layer, attrition and dentin sensitivity as well. Consequently, dental pulps were affected; thus, root canal treatments and pulpotomies were performed. In addition, the posterior teeth were crowned to preserve the remaining teeth structures and maintain the occlusion.

Moreover, missing teeth were #12, #22, #35, and #45 noticed in both siblings confirmed by the panorama (Fig. 2B i, j).

Increasingly, panorama revealed rectangular pulp chambers in relation to the upper dentitions as denoted by asterisks in Fig. 2B k. Taurodontism in the erupted molars was noticed as well (Fig. 2B k). Furthermore, several diffuse radiolucencies could be seen around

the anterior mandibular teeth in the male sibling (Fig. 2B k, l).

3.1.3. Family C

Three Pakistani siblings (IV-1, IV-2, and IV-5) (16-year-old male, 13-year and 8-year-old females) of family C manifested with the cardinal signs of the disorder; short stature, short trunk, brachyolmia, amelogenesis imperfecta, and hypodontia. Moreover, broad and wide foreheads, bulbous noses, short necks and broad chests were observed in the three patients, especially the female siblings. Further inquiry showed that they had normal psychomotor development with an average IQ of 90.

Intra-oral examination of all the affected individuals suggested hypodontia with severe attrition of the remaining teeth.

Table 1
Phenotypes of the patients in families A, B and, C.

Family ID	Family A		Family B		Family C		
Identified Gene Variants	*LTBP3*: c.3629-1G > T; p. ? *CABP2*: c.590T > C; p. Ile197Thr		*LTBP3*: c.132delG; p. Pro45Argfs*25		*LTBP3*: c.2216delG; p. Gly739Alafs*7		
Key phenotypic characteristics observed in patients of families A, B and C							
Patients	V-6	V-8	IV-1	IV-3	IV-1	IV-2	IV-5
Gender	Male	Female	Male	Female	Male	Female	Female
Ages (years)	25	18	13	8	16	13	8
Normal motor development	+	+	+	+	+	+	+
Short-stature	+	+	+	+	+	+	+
Short trunk	+	+	+	+	+	+	+
Back pain	–	–	+	+	–	–	–
Broad chest	+	–	–	–	+	+	+
Short neck	+	+	+	+	+	+	+
Occipito-frontal circumference (cm)	52 ± 1	52 ± 1	51	53	NA	NA	NA
Webbed neck	–	+	–	–	–	–	–
Hypertelorism	–	+	+	+	–	–	–
Hypotelorism	–	–	–	–	–	–	–
Short Philtrum	–	+	–	–	–	–	–
Scoliosis	+	+	–	–	–	–	–
Lordosis	–	–	–	–	–	–	–
Kyphosis	–	–	–	–	–	–	–
Clinodactyly	+	+	–	–	–	–	–
Pes planus	+	+	–	–	NA	NA	NA
Yellow-brown discoloration of teeth	+	+	–	–	+	+	+
Yellow discoloration of teeth	–	–	+	+	–	–	–
Attrition	+	+	++	++	++	++	++
Spacing of teeth	+	+	+	+	+	++	++
Hypodontia	+	+	+	+	+	+	+
Enamel	Absent	Absent	Thin	Thin	Absent	Absent	Absent
Dentine reduced	+	+	–	–	+	+	+
Dentine sensitivity	+	+	+	+	+	+	+
Hypertaurodont	–	–	+	–	–	–	–
Amelogenesis imperfecta	+	+	+	+	+	+	++
Gingivitis	–	–	–	–	–	–	+
Root canal treatment	+	+	+	+	–	–	–
Spine anomalies	+	+	+	+	NA	NA	NA
Reduced disc space	+	+	+	+	NA	NA	NA
Flat and biconcave rectangular vertebrae	+	+	+	+	NA	NA	NA
Broad/round vertebral bodies	+	+	+	+	NA	NA	NA
Brachyolmia	+	+	+	+	+	+	+
Spinal stenosis	+	+	+	+	NA	NA	NA
Osteopenia	–	–	+	+	NA	NA	NA
Subchondral cysts at the head of the femur and acetabulum	+	+	–	–	NA	NA	NA
Calcification at the head of the femur and acetabulum	+	+	–	–	NA	NA	NA
Epiphyseal ossification of femurs	+	+	–	–	NA	NA	NA
Bilateral narrow joint spaces in hips	+	+	+	+	NA	NA	NA
Tibial deformity	–	–	+	+	NA	NA	NA
Joint changes	–	–	–	–	NA	NA	NA
Short limbs, hands, and feet	–	–	+	+	+	+	+
Short distal phalanges	+	+	+	+	+	+	+
Ocular abnormalities	–	–	–	–	–	–	–
Bilateral hearing impairment	+	+	–	–	–	–	–
Speech impairment	–	–	–	–	–	–	–
Interatrial/atrial septal aneurysm (ASA)	–	–	+	–	NA	NA	NA
Dilation of ascending aorta	–	–	+	–	NA	NA	NA
Secundum atrial septal defect (ASD)	–	–	–	+	NA	NA	NA

Footnotes: ++ shows severe condition, NA: Not applicable because of the unavailability of the skeletal X-rays.

Furthermore, all teeth were widely spaced, especially in patients IV-1 and IV-5. The weakened severely affected enamel caused early loss of occlusal/incisal anatomy and attrition. Furthermore, generalized enamel loss in both primary and permanent dentitions, leading to several teeth sensitivity, with pulp exposure in some teeth. All dentitions had yellow-brown discoloration with diffuse pitted enamel surface in the examined patients. Additionally, the three siblings (IV-1, IV-2, and IV-5) had multiple retained teeth. Normal gingival appearance and contouring were seen in patients IV-1, IV-2, although IV-5 was observed with marginal gingivitis (Fig. 2C a, b, c).

Furthermore, bone height was reduced in several areas, especially premolar regions. The younger female sibling (IV-5) had a severe form of amelogenesis imperfecta (Fig. 2C d, e, f). Panoramic radiographs of the affected siblings revealed multiple dentitions agenesis, especially in the younger female sibling (IV-5), who had hypodontia in #22 and #45.

A phenotype comparison of all the patients in three families A, B and, C are enlisted in Table 1.

3.1.4. Variant identification and Co-segregation analysis in families A, B, and C

While analyzing the exome data of family A, several ROH residing on chromosomes 11q13.1, 11q13.2, 11q14.1, 2p11.2, 12p13.33, and 12p13.31 were identified. These chromosomal locations harbour eight rare variants including, (*LTBP3*; NM_001130144.2, c.3629-1G > T; p. ?) in (11q13.1), (*CABP2*; NM_016366.3; c.590T > C; p.Ile197Thr) in (11q13.2), (*ODZ4/TENM4*; NM_001098816.2, c.55G > C; p.Glu19Gln), (*TMEM126B*; NM_018480.4, c.397+1G > A; p. ?), and (*TMEM126B*; NM_001256546.1, c.308-7T > A; p. ?) in (11q14.1), (*KDM3A*; NM_018433.5, c.2291C > T; p.Pro764Leu) in (2p11.2), (*C12orf32/RHNO1*; NM_001257098.1, c.470T > C; p. Ile157Thr) in (12p13.33), and (*VWF*; NM_000552.3, c.1892C > T; p.Ala631Val) in (12p13.31) (Suppl. Table 2). Using the variant validation criteria mentioned in the materials and methods section, we found no rare variants other than those enlisted in Suppl. Table 2. Hence, the variants mentioned above were preferred for the co-segregation analysis.

We also tested the in-house hearing impairment gene panel, which includes autosomal dominant, recessive, and X-linked genes involved in syndromic and non-syndromic deafness, but we could not find any other variant except that of *CABP2* in family A.

According to the ACMG variant classification guidelines, the *LTBP3* (c.3629-1G > T; p. ?) and *TMEM126B* (c.397+1G > A; p. ?) variants fulfilled the criteria of being pathogenic and likely pathogenic, respectively. The *CABP2* variant (c.590T > C; p.Ile197Thr) was declared presumably benign following the ACMG guidelines. Interestingly, neither the *TMEM126B* variant nor the other likely benign

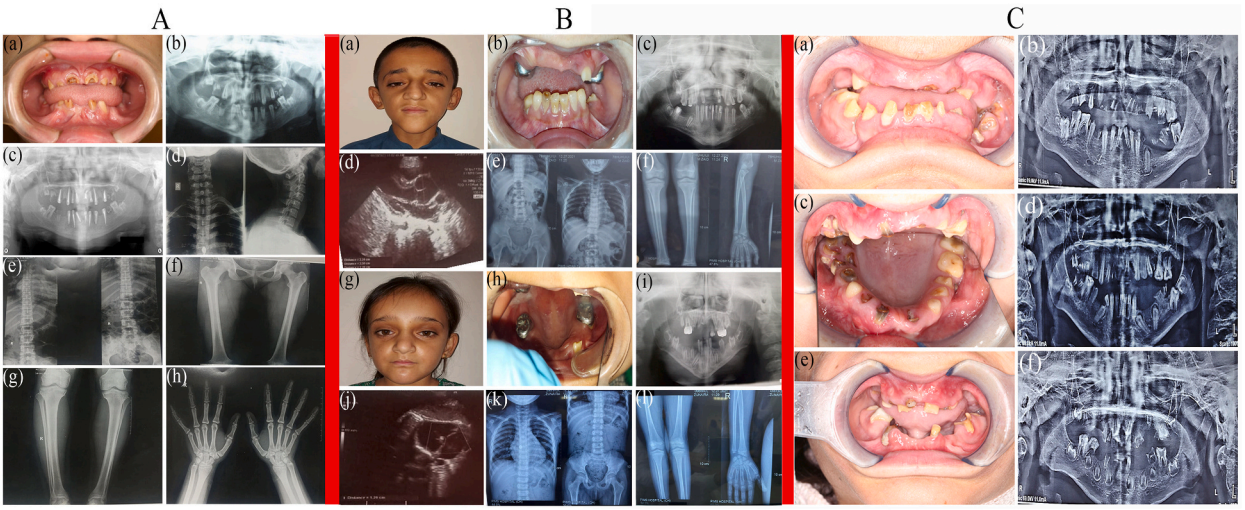

Fig. 2. (A) Clinical phenotypes of family A. (a) and (b) The spine X-rays showing biconcave rectangular vertebrae and narrow disc space between vertebrae, the characteristic features of brachyolmia. (c) Hip X-ray demonstrating the bilateral narrow joint space and protrusion of both hips. (d) Lower limb X-ray showing both limbs' bilateral thick cortex and mild bowing. (e) Hand X-ray showing the short distal phalanges. (f) The dentition of the affected individual showing destructed yellowish brown discoloration with spacing. (g) Represent the pre-operative panoramic view of the affected individual. (h) Post-operative panoramic view after dental treatment of the necrotic teeth.
(B) Clinical features of family B. (a) and (b) show facial features of patient-IV-1 and -IV-3 showing oval-faced shapes, broad and wider foreheads, thin almond and monolid eyes, bulbous noses, pointed chins, and attached earlobes. (c) Spine and hip X-rays showing the widened vertebral bodies rounded anterior surface, short pedicles with narrow inter-vertebral discs space, protrusion of both the hips, narrow hip joint spaces and coxa valga. (d) Lower limb and upper limb X-rays revealing normal joints and shortened distal phalanges. (e) Spine and hip X-rays of patient-IV-3 showing widened vertebral bodies with rounded anterior surfaces. (f) Lower limb and upper limb X-rays showing normal joints and shortened distal phalanges. (g) and (h) Transthoracic echocardiogram confirms the interatrial septal aneurysm or atrial septal aneurysm (ASA) and atrial septal defect (ASD) secundum with IVS paradox. (i) and (j) Intraoral photographs of mild hypoplastic enamel of the teeth of patient-IV-1 and severe form of tooth attrition and agenesis of patient-IV-3. (k) and (l) OPGs showing the congenital absence of teeth #12, #22, #35, and #45 in both patients. (C) Photographs of family C. (a) Intraoral photograph showing loss of enamel layer and yellowish discolored dentition of patient-IV-1. (b) Intraoral photograph showing badly destructed teeth with amelogenesis imperfecta in patient IV-2. (c) Intraoral photograph showing badly destructed teeth with amelogenesis imperfecta. (d) Panoramic radiograph of patient-IV-1 showing congenital missing teeth. (e) Panorama showing congenitally missing teeth of patient-IV-2. (f) OPG of patient-IV-5, denoting hypodontia of #22 and #45.

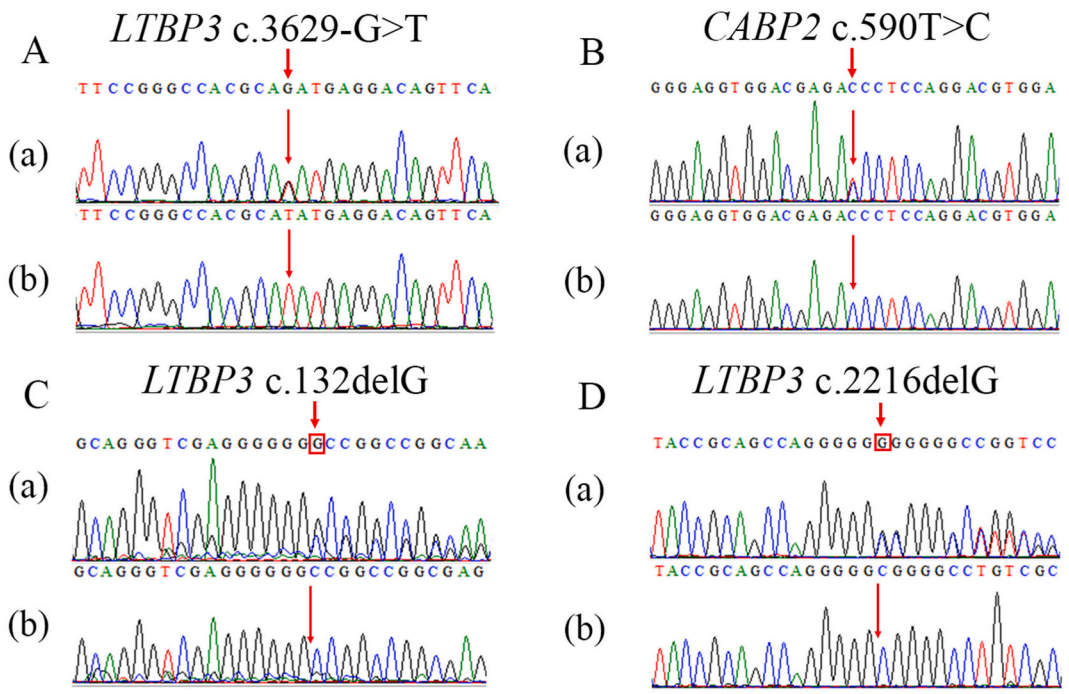

Fig. 3. (A) Tympanogram of the left ear, and (b) tympanogram of the right ear of affected individual V-6. (c) and (d) tympanograms of the left and right ears, respectively, of affected individual V-8 in family-A.

variants and the variants of unknown significance are segregated in the family (Suppl. Table 3). However, the *LTBP3* and *CABP2* variants, located on chromosome 11q13.1 and 11q13.2 respectively, are segregated in family A. In addition, the *LTBP3* and *CABP2* variants achieved the significant CADD scores of 33 and 25.2, respectively (Suppl. Table 3).

The exome analysis identified two recurrent frameshift variants, c.132delG; p.Pro45Argfs*25 in exon-1 and c.2216delG; p. Gly739Alafs*7 in exon-15 of the *LTBP3* in families B and C, respectively. Later, the Sanger sequencing analysis confirmed the co-segregation of these variants in the respective families (Fig. 4 A, B, C, and D).

4. Discussion

In this study, we report a novel pathogenic splice acceptor site variant (c.3629-1G > T; p. ?) in *LTBP3* and a missense variant (c.590T > C; p.Ile197Thr) in *CABP2* gene in an Egyptian family, along with two recurrent frameshift variants (c.132delG; p. Pro45Argfs*25 and c.2216delG; p.Gly739Alafs*7) in *LTBP3* in two Pakistani families. The causative *LTBP3* and *CABP2* variants were first identified through exome sequencing and then validated by Sanger sequencing.

In case of splice acceptor site variant (c.3629-1G > T; p. ?) in family A, an alteration takes place in the sequence of intron-26 (at the 3′ end). This alteration replaces CAG sequence with CAT in the constitutive splice site acceptor region (SSA) before exon-27 of the *LTBP3* gene that likely alters the SSA. The outcome of the c.3629-1G > T; p. ? variant is predicted, the skipping of exon-27, resulting in the deletion of the 44 amino acids (1210–1253), which compose the EGF-like Ca^{++}-binding domain-13 (EGF-CBD13) of the LTBP3 protein. As a result, a non-functional LTBP3 protein consisting of 1259 amino acids will be produced. In addition, it may also activate the nonsense-mediated mRNA decay (NMD), leading to partial or complete elimination of the *LTBP3* mRNA transcript. Both the patients (V-6 and V-8) in family A are homozygous, while the mother (IV-6) is heterozygous for this splice site variant c.3629-1G > T; p. ? (Fig. 4A a, b). However, the splice site prediction tool, the varSEAK (https://varseak.bio/), categorized this variant (c.3629-1G > T; p. ?) as a variant of the Class-5 splicing effect. It also predicted that the variant would result in exon skipping with no AG (Adenine, Guanine at the 3′ end of intron 26, i.e., splice acceptor site) retention and loss of function (Suppl. Table 3).

To date, five splice site *LTBP3* variants including; c.3107-2A > G; p.? [6], c.1721-2A > G; p.? [5], c.1531+1G > T; p. ? [9], c.2894-2A > G; p. ?) [3] and, c.1846+5G > A; p. ? [24] have been reported in the literature. The first four variants cause DASS phenotypes, while the fifth causes GPHYSD3 phenotypes. In addition, these splice site variants have been predicted and verified to activate the NMD machinery and could decrease protein levels [3,5,25].

Patients in family A presented DASS in addition to specific phenotype including short and webbed necks, broad chests, pes planus, subchondral cysts, and abnormal calcification at the head of the femur and acetabulum which are not enlisted in previous publications with *LTBP3* splice site variants (Table 2). In addition, some specific phenotypes reported previously in various publications of already identified *LTBP3* splice site variants, were not observed in our patients (Table 2). However, the new findings in our patients presented with short and webbed necks, broad chests, pes planus, reduced disc space, flat and biconcave rectangular vertebrae, broad/round

vertebral bodies, subchondral cysts and calcification at the head of the femur and acetabulum, epiphyseal ossification of femurs, bilateral narrow joint spaces in hips and bilateral hearing impairment (Table 2). It is essential to mention that the loss of various domains and the formation of aberrant proteins of different sizes may cause phenotypes variations.

Furthermore, the studies conducted so far on the involvement of *LTBP3* in humans in various phenotypes have shown no association between *LTBP3* and hearing loss; however, when *Ltbp3*expression in the developing mouse embryos was analyzed by performing *in situ* hybridization, a discrete expression of *Ltbp3* was observed in the developing inner ear (cochlea) [9]. Even then, we believe that the *CABP2* variant (NM_016366.3: c.590T > C; p.Ile197Thr) in exon-6 is causing hearing impairment in family A. The mother (IV-6) was heterozygous, while both the patients (V-6 and V-8) with autosomal recessive hearing loss were homozygous for the missense variant (Fig. 4B a, b). The identified *CABP2* missense variant (c.590T > C; p.Ile197Thr; rs145369252) has already been reported in the Iranian population for autosomal recessive hereditary hearing loss [26]. CABP2 plays a critical role in encoding sound waves at inner hair cells (IHCs) synapses by inhibiting the inactivation of voltage-gated Ca^{++} channel of type 1.3 (CaV 1.3) in the IHCs [27].

Patients IV-1 and IV-3 in family B with DASS and aortopathy phenotypes showed the homozygous frameshift variant c.132delG; p.Pro45Argfs*25 while the father (III-2) was heterozygous for the *LTBP3* variant and did not present DASS or aortic disease symptoms (Fig. 4C a, b). This variant is located downstream of the signal peptide (1–43 amino acids) in the LTBP3 protein. This 1-bp deletion causes a frameshift and premature truncation after 25 amino acids. As a result, a truncated mutant LTBP3 protein consisting only of 68 amino acids is produced compared to the full-length wild-type LTBP3 protein (1303 amino acids), which leads to delete a large portion of the LTBP3 (1235 amino acids) protein. This homozygous frameshift deletion leads to the eradication of core domains of the encoded protein, including EGF-like Ca^{++} binding domains, EGF-like non-Ca^{++} binding domains and TGF-β binding domains (8-Cys domains), causing loss-of-function of the LTBP3. Amelogenesis imperfecta, short stature, arterial aneurysm, and aortic root dilation demonstrated

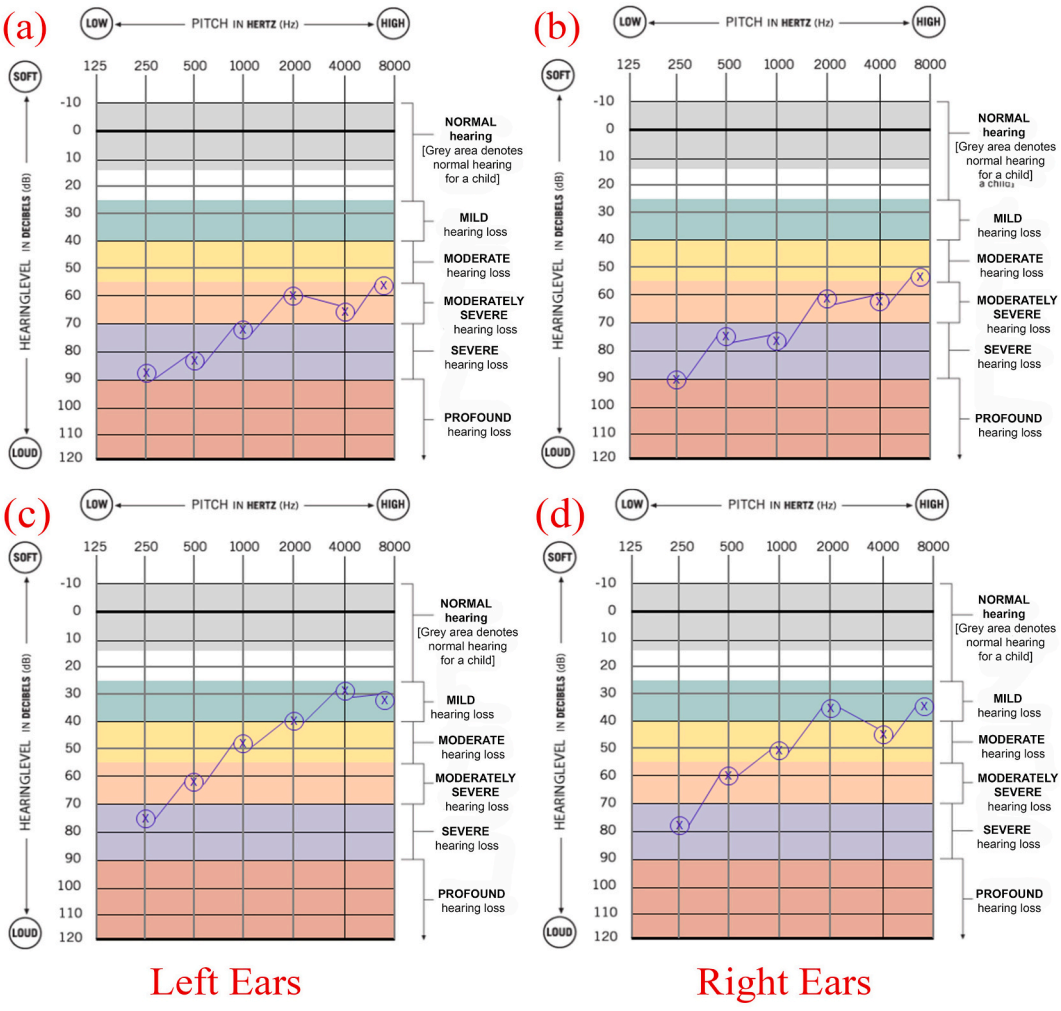

Fig. 4. Sequencing Chromatograms. (A, b) Chromatograms of the parent (IV-6) and affected individual (V-6) in *LTBP3* variant in family A. (B a, b) Chromatograms of the parent (IV-6) and affected individuals (V-6) in *CABP2* variant in family A. (C a, b) Chromatograms of the parent (III-2) and affected individual (IV-1) in *LTBP3* variant in family B. (D a, b) Chromatogram of the parent (III-2) and affected individual (IV-1) in *LTBP3* variant in family C.

Table 2
Phenotypes comparison of the patients in families A and previously reported patients carrying splice site variants.

Studies Conducted		Kantaputra et al., 2022				Flex et al., 2021	Intarak et al., 2019	McInerney-Leo et al., 2016		Huckert et al., 2015		Current Stud	
Identified *LTBP3* Variants		(c.3107-2A > G)				(c.2894-2A > G)	(c.1721-2A > G)	(c.1846+5G > A)		(c.1531+1G > T)		(c.3629-1G > T)	
Likely Lost/affected LTBP3 Domains													
Domains		EGF-like Ca++-binding domain-11 (EGF-CBD11)				TGF-β-binding domain-3	EGF-like domain-3	EGF-like domain-3		TGF-β-binding domain-2		EGF-like Ca^{++}-binding domain-13 (EGF-CBD13)	
Family No./ID		1				1	2	Unrelated GD patients		2		A	
Consanguinity		–				+	+	–		–		+	
Patients		1	2	3	4	1	1	GD-1	GD-2	1	2	V-6	V-8
Gender		F	F	M	M	M	F	M	M	F	M	M	F
Ages (years)		19	44	52	20	14	24	4				25	18
Standing Heights (cm)		155	156	159	177	52	140	60.5	65.5	NR	NR	146 ± 1	137.5 ± 1
PHENOTYPES OF THE PATIENTS	Occipito-frontal circumference (cm)	55	NR	NR	NR	NR	NR	49.5	48.5	NR	NR	52 ± 1	52 ± 1
	Normal motor development	+	+	+	+	+-	+	+	+	NR	NR	+	+
	Short neck	–	–	–	–	–	–	–	–	–	–	+	+
	Webbed neck	–	–	–	–	–	–	–	–	–	–	+	
	Broad chest	–	–	–	–	–	–	–	–	–	–	+	–
	Facial dysmorphisms	+	–	+	–	+	–	+	–	–	–	–	–
	Biparietal bossing	+	–	–	–	–	–	–	–	–	–	–	–
	Hypertelorism	–	–	–	–	–	–	–	–	+	–	–	+
	Recurrent bronchiolitis	–	–	–	–	–	–	+	–	–	–	–	–
	Short hands and feet	–	–	–	–	–	–	+	+	–	–	–	–
	Thick skin, hepatomegaly and permanent dyspnoea	–	–	–	–	–	–	+	+	–	–	–	–
	Delayed bone age	–	–	–	–	–	–	+	–	–	–	–	–
	Stiff joints	–	–	–	–	–	–	–	+	–	–	–	–
	Epiphyseal dysplasia at the upper femoral region	–	–	–	–	–	–	+	–	–	–	–	–
	Cone-shaped epiphyses	–	–	–	–	–	–	–	+	–	–	–	–
	Short hands and feet	–	–	–	–	–	–	+	+	–	–	–	–
	Tracheal stenosis	–	–	–	–	–	–	+	–	–	–	–	–
	Sleep apnoea	–	–	–	–	–	+	+	+	–	–	–	–
	Alveolo-interstitial pneumonia	–	–	–	–	–	–	+	+	–	–	–	–
	Pulmonary hypertension	–	–	–	–	–	–	+	–	–	–	–	–
	Dyspnoea	–	–	–	–	–	–	+	+	–	–	–	–
	Oesophageal reflux	–	–	–	–	–	–	–	+	–	–	–	–
	Vertebral osteopenia	+	–	–	–	–	–	–	–	+	–	–	–
	Maxillary hypoplasia	–	+	–	–	–	–	–	–	–	–	–	–
	Abnormal dentin	+	–	–	–	–	–	–	–	–	–	–	–
	Calcified dental pulp blood vessels	+	–	–	–	–	–	–	–	–	–	–	–
	Taurodontism	+	–	–	–	–	–	–	–	+	–	–	–
	Hypertaurodontism	–	–	–	–	–	–	–	–	–	–	–	–
	Root canal treatment	–	–	–	–	–	–	–	–	–	–	+	+
	Single-rooted molars	+	–	–	–	–	–	–	–	–	–	–	–
	Failure of mandibular tooth eruption	+	–	–	–	–	–	–	–	–	–	–	–

(*continued on next page*)

Table 2 (*continued*)

Studies Conducted	Kantaputra et al., 2022				Flex et al., 2021	Intarak et al., 2019	McInerney-Leo et al., 2016		Huckert et al., 2015		Current Stud	
Irregular posterior bone	+	–	–	–	–	+	–	–	–	–	–	–
Prognathic mandible	+	–	–	–	–	–	–	–	–	–	–	–
Secundum atrial septal defect (ASD)	+	–	–	–	–	–	–	–	–	–	–	–
Interatrial septal aneurysm (ASA)	+	+	–	–	–	–	–	–	–	–	–	–
Aortic root dialation	+	+	–	–	–	–	–	–	–	–	–	–
Hypertrophic cardiomyopathy	–	–	–	–	+	–	–	–	–	–	–	–
Mild mitral and mild tricuspid valve regurgitations	+	–	–	–	–	–	–	–	–	–	–	–
A recurrent glenohumeral joint dislocation	+	–	–	–	–	–	–		–		–	–
Clinodactyly	+	–	–	–	–	–	–	–	–	–	+	+
Brachydactyly	+	–	–	–	–	–	+	+	–	–	–	–
Amelogenesis imperfecta	+	–	–	–	+	+	+	+	+	+	+	+
Yellow-brown discoloration of teeth	–	–	–	–	–	–	–	–	–	–	+	+
Yellow teeth discoloration of teeth	+	–	–	–	+	+	+	+	+	+	–	–
Hypodontia	+	–	–	–	+	+	–	–	–	–	+	+
Microdontia	+	–	–	–	+	+	+	+	+	+	–	–
Spacing of teeth		–	–	–	+		+	+	+	+	+	+
Short stature	+	+	+	+	+	+	+	+	+	+	+	+
Short trunk	–	–	–	–	+	–	–	–	–		+	+
Brachyolmia	+	–	–	–	+	+	+	+	+	+	+	+
Abnormal dentin	+	–	–	–	–	–	–	–	–	–	–	–
Dentine reduced	–	–	–	–	–	–	–	–	–	–	+	+
Dentine sensitivity	–	–	–	–	–	–	–	–	–	–	+	+
Short philtrum	+	–	–	–	–	–	–	–	–	–	–	+
Long philtrum	–	–	–	–	–	+	–	–	–	–	–	–
Absent enamel	+	–	–	–	–	–	+	+	+	–	+	+
Thin enamel	–	–	–	–	–	–	–	–	+	–	–	–
Enamel hypoplasia	–	–	–	–	–	–	–	–	+	–	–	–
Attrition	–	–	+	–	–	–	–	–	–	–	+	+
Normal dentine	+	+	+	+	–	–	–	–	+	–	–	–
Reduced radiopacity	–	–	–	–	+	–	–	–	–	–	–	–
Large pulp chambers	–	–	–	–	–	–	+	+	+	–	–	–
Taurodontic in molars	–	–	–	–	–	–	+	+	+	–	–	–
Mandibular prognathism	–	+	+	–	–	–	+	+	+	–	–	–
Microstomia	–	–	–	–	–	+	–	–	–	–	–	–
Platyspondyly	–	–	–	–	+	–	–	–	–	–	–	–
Lumbar lordosis	–	–	–	–	–	+	–	–	–	–	–	–
Scoliosis	–	–	–	–	+	–	–	–	+	–	+	+
Pterygium colli	–	–	–	–	+	–	–	–	–	–	–	–
Varus knees	–	–	–	–	+	–	–	–	–	–	–	–
Lower limbs diplegia	–	–	–	–	+	–	–	–	–	–	–	–
Valvular aortic stenosis	–	–	–	–	+	+	–	–	–	–	–	–
Short hands, feet, fingers, and toes	–	–	–	–	–	+	–	–	–	–	–	–
Short hands and feet	–	–	–	–	–	–	+	+	–	–	–	–
Short distal phalanges	–	–	–	–	–	–	–	–	–	–	+	+
Pes planus	–	–	–	–	–	–	–	–	–	–	+	+
Brachydactyly	+	–	–	–	+	–	–	–	–	–	–	–
Widened proximal epiphyseal region of the tibiae	–	–	–	–	+	–	–	–	–	–	–	–
Widened distal epiphyseal region of the femurs	–	–	–	–	+	–		–	–	–	–	–

(*continued on next page*)

Table 2 (*continued*)

Studies Conducted		Kantaputra et al., 2022				Flex et al., 2021	Intarak et al., 2019	McInerney-Leo et al., 2016		Huckert et al., 2015		Current Stud	
	Reduced disc space	–	–	–	–	–	–	–	–	–	–	+	+
	Flat and biconcave rectangular vertebrae	–	–	–	–	–	–	–	–	–	–	+	+
	Broad/round vertebral bodies	–	–	–	–	–	–	–	–	–	–	+	+
	Spinal stenosis	–	–	–	–	–	–	–	–	–	–	+	+
	Subchondral cysts at the head of the femur and acetabulum	–	–	–	–	–	–	–	–	–	–	+	+
	Calcification at the head of the femur and acetabulum	–	–	–	–	–	–	–	–	–	–	+	+
	Epiphyseal ossification of femurs	–	–	–	–	–	–	–		–	–	+	+
	Bilateral narrow joint spaces in hips	–	–	–	–	–	–	–		–	–	+	+
	Tibial deformity	–	–	–	–	–	–	–		–	–	–	–
	Bilateral hearing impairment	–	–	–	–	–	–	–		–	–	+	+
	Ocular abnormalities	–	–	–	–	–	–	–		–	–	–	–
	Hair anomalies	–	–	–	–	–	–	–	–	–	–	–	–
	Nail anomalies	–	–	–	–	–	–	–	–	–	–	–	–
	Speech impairment	–	–	–	–	–	–	–		–	–	–	–

Table 3
Phenotypes comparison of the patients in families B and C, and the previously reported patients carrying the same LTBP3 variants.

Studies Conducted		Guo et al., 2018			Current Study		Huckert et al., 2015	Current Study		
Identified *LTBP3* Variants		c.132delG; p. Pro45Argfs*25			c.132delG; p. Pro45Argfs*25		c.2216delG; p.Gly739Alafs*7	c.2216delG; p. Gly739Alafs*7		
Likely Lost/affected LTBP3 Domains										
Domains		All domains i.e. EGF-like Ca^{++} binding domains, EGF-like non-Ca^{++} binding domains and TGF-β binding domains (8-Cys domains)			All domains i. e. EGF-like Ca^{++} binding domains, EGF-like non-Ca^{++} binding domains and TGF-β binding domains (8-Cys domains)		Eight EGF-like Ca^{++} binding domains (EGF-CBD6-13) and two TGF-β binding domains (TB-3 and -4)	Eight EGF-like Ca^{++} binding domains (EGF-CBD6-13) and two TGF-β binding domains (TB-3 and -4)		
Family No./ID		TAA909			B		3	C		
Consanguinity		–			+		+	+		
Patients		III-2	III-3	III-4	IV-1	IV-3	1	IV-1	IV-2	IV-5
Gender		F	M	F	M	F	M	M	F	F
Ages (years)		59	54	55	13	8	NR	16	13	8
Standing Heights		147	160	152	126 ± 1	112 ± 1	NR	NR	NR	NR
PHENOTYPES OF THE PATIENTS	Occipito-frontal circumference (cm)	NR	NR	NR	51	53	NR	NA	NA	NA
	Normal motor development	NR	NR	NR	+	+	+	+	+	+
	Abdominal aortic aneurysm	–	+	–	–	–	–	–	–	–
	Aortic root dilation	–	+	+	+	–	–	–	–	–
	arterial aneurysms: axillary, iliac, hepatic, celiac axis	–	+	–	–	–	–	–	–	–
	Interatrial/atrial septal aneurysm (ASA)	–	–	–	+	–	–	NA	NA	NA
	Dilation of ascending aorta	–	–	–	+	–	–	NA	NA	NA
	Secundum atrial septal defect (ASD)	–	–	–	–	+	–	NA	NA	NA
	Amelogenesis imperfecta	+	+	+	+	+	+	+	+	++
	Brachyolmia	–	–	–	+	+	+	+	+	+
	Cataracts	–	+	–	–	–	–	–	–	–
	Mitral valve prolapse	+	–	+	–	–	–	–	–	–
	Mitral valve, tricuspid valve regurgitation	+	–	–	–	–	–	–	–	–
	Diffuse sclerosis of thoracic spine	+	–	–	–	–	–	–	–	–
	Osteoporosis	+	–	–	–	–	–	–	–	–
	Femur fracture	+	–	–	–	–	–	–	–	–
	Short stature	+	+	+	+	+	+	+	+	+
	Reduced disc space	–	–	–	+	+	–	NA	NA	NA
	Yellow-brown discoloration of teeth	–	–	–	–	–	–	+	+	+
	Yellow discoloration of teeth	+	–	–	+	+	+	–	–	–
	Microdontia	–	–	–	–	–	+	–	–	–
	Gingivitis	–	–	–	–	–	–	–	–	+
	Teeth spacing	–	–	–	+	+	+	+	++	++
	Large pulp chambers	–	–	–	–	–	+	–	–	–
	Root canal treatment	–	–	–	+	+	–	–	–	–
	Taurodontism	–	–	–	–	–	+	–	–	–
	Hypertaurodontism	–	–	–	+	–	–	–	–	–
	Thin enamel	–	–	–	+	+	–	–	–	–
	Absence of enamel	–	–	–	–	–	+	+	+	+
	Dentine reduced	–	–	–	–	–	–	+	+	+
	Dentine sensitivity	–	–	–	+	+	–	+	+	+
	Mandibular prognathism	–	–	–	–	–	+	–	–	–
	Retarded teeth eruption	–	–	–	–	–	+	–	–	–
	Back pain	–	–	–	+	+	–	–	–	–
	Attrition	–	–	–	++	++	–	++	++	++
	Hypodontia	–	–	–	+	+	–	+	+	+
	Short trunk	–	–	–	+	+	–	+	+	+
	Broad chest	–	–	–	–	–	–	+	+	+
	Short neck	–	–	–	+	+	–	+	+	+
	Hypertelorism	–	–	–	+	+	–	–	–	–

(*continued on next page*)

Table 3 (*continued*)

Studies Conducted		Guo et al., 2018			Current Study			Huckert et al., 2015	Current Study		
	Flattened and biconcave rectangular vertebrae	–	–	–	+	+	+	NA	NA	NA	
	Broad/round vertebral bodies	–	–	–	+	+	–	NA	NA	NA	
	Spinal stenosis	–	–	–	+	+	–	NA	NA	NA	
	Osteopenia	–	–	–	+	+	–	NA	NA	NA	
	Short limbs, hands, and feet	–	–	–	+	+	–	+	+	+	
	Short distal phalanges	–	–	–	+	+	–	+	+	+	
	Bilateral narrow joint spaces in hips	–	–	–	+	+	–	NA	NA	NA	
	Tibial deformity	–	–	–	+	+	–	NA	NA	NA	
	Ocular abnormalities	–	–	–	–	–	–	–	–	–	
	Bilateral hearing impairment	–	–	–	–	–	–	–	–	–	
	Speech impairment	–	–	–	–	–	–	–	–	–	
	Nail anomalies	–	–	–	–	–	–	–	–	–	
	Hair anomalies	–	–	–	–	–	–	–	–	–	

Foot Notes: NR; Not reported, NA; Not applicable, ++; more severe, F; female, M; male.

by the patients of family B were consistent with the phenotypes of the patients reported by Guo et al. [4]. The other phenotypes listed in this publication were not observed in our patients (Table 3). The differences in phenotypes between Guo et al. and family B variant may be because of compound monoallelic variants (*LTBP3*:c.2248G > T; p.Glu750*, *LTBP3*:c.132delG; p.Pro45Argfs*25) in Guo et al. [4] study and homozygous variant (*LTBP3*:c.132delG; p.Pro45Argfs*25) in our study.

In patients IV-1, IV-2, and IV-5 of family C, a homozygous frameshift variant c.2216delG; p.Gly739Alafs*7 was identified in exon-15 of the *LTBP3* (Fig. 4D a, b). This variant is located between the EGF-like non-Ca^{++} binding domains-5 and -6. This 1-bp deletion is predicted to cause a frameshift and premature truncation after seven amino acids. As a result a truncated mutant LTBP3 protein consisting only of 744 amino acids is produced, and a large portion of the protein (559 amino acids) is deleted. This homozygous frameshift deletion eliminates eight EGF-like Ca^{++} binding domains (EGF-CBD6-13), and two TGF-β binding domains (TB-3 and -4). Previously, this variant has been reported by Huckert et al. in a family of Brazilian origin with DASS phenotypes; short stature, amelogenesis imperfecta, delayed eruption of teeth, and mild platyspondyly (brachyolmia) [9]. Similarly, families B and C consistently demonstrated short stature, amelogenesis imperfecta, teeth spacing, and brachyolmia (Table 3). However, they additionally presented some novel phenotypes, which, according to our knowledge, are not documented in the previously reported patients with *LTBP3* frameshift mutations. These exceptional phenotypes include; back pain, hypertelorism, short neck, broad chests, and tibial deformity (Table 3). We conclude that the same type of variants are causing different phenotypes in different populations. Moreover, the phenotypes of the patients studied by Guo et al. and Huckert et al. [4,9] revealed the significant range of phenotypic variations (Table 3).

Studies on $Ltbp3^{-/-}$ knockout mice have proved LTBP3 as a regulator in the bioavailability of TGF-β in chondrocytes. LTBP3 is essential for TGF-β signaling, as LTBP3-lacking mice had long bone deformities similar to those with abnormal TGF-β signaling [28]. Similarly, studies on *Ltbp3* null mice showed that they were more than 50 % smaller than the wild-type mice with dental and skeletal malformations [29]. Furthermore, Noor et al. have identified a pathogenic mutation in *LTBP3*, causing oligodontia in the Pakistani population [7]. These abnormalities are the outcomes of aberrant TGF-β signaling because of the following observations from previous researchers. TGF-β and bone morphogenetic protein (BMP) signalings have fundamental roles in osteoblast differentiation, embryonic skeletal development, and bone formation [30]. Without TGF-β signalling, smooth muscle cells cannot differentiate into quiescent cells [31]. The abnormal TGF-β signalling causes aneurysm development in many diseases [32]. The secundum atrial septal defect and atrial septal aneurysm are caused by the *LTBP3* variants because the TGF-β-BMP signalling disturbance that is essential for the development of atrioventricular septal complex and septum primum [33]. Based on these facts, it can be generalized that *LTBP3* is vital for skeletal, tooth and heart development. In all the frameshift and splice site mutations, the LTBP3 protein lacks the essential functional domains, which leads to failure of the TGFβ–LAP–LTBP3 complex formation and eventually will disturb TGF-β secretion and activation. In intact form, the TGFβ–LAP–LTBP3 complex is necessary for proper folding and secretion of TGF-β [34].

In conclusion, we find significant phenotypic variations among patients of the enrolled families (A, B, C) in this study and among our patients and those reported in previous studies. The phenotypic variability in monogenic disorders may be dependent on population types coming from various geographical locations [35], mutation type and its location in the gene [36,37], and loss of or defective functional domains of the protein [38,39]. The different phenotypes in the same gene are also thought to be caused by other factors, including common variants, variants in regulatory regions, epigenetics, and environmental factors [40].

We have performed thorough clinical and molecular investigations in this study but could not establish genotype-phenotype correlation. The recruitment of further patients carrying *LTBP3* variants and future functional studies using animal models may explain the phenotypic variability among the patients to establish genotype-phenotype correlation.

Ethics declarations

The ethical committee of the National Research Centre (Local project 12060202), Cairo, Egypt, and the research and ethical committee (certificate no. 1998) of Kohat University of Science and Technology, Kohat, Pakistan, approved the study. The participants

and legal guardians, in case of minors, provided informed consent to participate in the study. They also consented to publish their clinical data, including the photographs, for a scientific publication.

Data availability

The data of this study has been submitted to a public repository ClinVar (https://www.ncbi.nlm.nih.gov/clinvar/) under the accession numbers SCV002599103, SCV004171027, SCV004171028, and SCV004171029.

Funding

Naveed Wasif got the research support from the George Förster Fellowship (2015–2018) of the Alexander von Humboldt Foundation, Bonn, Germany. The Higher Education Commission (HEC), Islamabad, Pakistan, partly supported the work through NRPU project (No.5890/NRPU/R&D/HEC 2016).

The laboratory investigations, panoramas, skeletal surveys, eye examination, heart echo and hearing testing of family A were funded by the local project of National Research Centre (NRC), Cairo, Egypt (No#12060202).

CRediT authorship contribution statement

Hamed Nawaz: Investigation, Writing – original draft. **Asia Parveen:** Data curation, Formal analysis, Methodology. **Sher Alam Khan:** Data curation, Formal analysis, Methodology, Writing – original draft. **Abul Khair Zalan:** Investigation. **Muhammad Adnan Khan:** Investigation. **Noor Muhammad:** Conceptualization, Writing – review & editing. **Nehal F. Hassib:** Funding acquisition, Investigation, Writing – review & editing. **Mostafa I. Mostafa:** Investigation, Writing – review & editing. **Rasha M. Elhossini:** Investigation, Writing – original draft, Writing – review & editing. **Nehal Nabil Roshdy:** Investigation. **Asmat Ullah:** Data curation, Investigation. **Amina Arif:** Supervision, Writing – original draft. **Saadullah Khan:** Supervision, Writing – review & editing, Conceptualization, Funding acquisition. **Ole Ammerpohl:** Writing – review & editing. **Naveed Wasif:** Conceptualization, Data curation, Formal analysis, Methodology, Writing – original draft, Writing – review & editing.

Declaration of competing interest

The authors declare the following financial interests/personal relationships which may be considered as potential competing interests:Naveed Wasif reports financial support was provided by Alexander von Humboldt Foundation. Saadullah Khan reports financial support was provided by Higher Education Commission Pakistan. Nehal F. Hassib reports financial support was provided by National Research Centre, Cairo. The authors declare that they have no competing interests.

Acknowledgements

We are grateful to the research volunteers for their participation and cooperation in this study. We are thankful to Prof. Reiner Siebert, Institute of Human Genetics, Ulm University and Ulm University Medical Center, 89081, Ulm, Germany, for his support during the study. We acknowledge the financial support by DFG within the funding programme Open Access-Publikationskosten.

Appendix A. Supplementary data

Supplementary data to this article can be found online at https://doi.org/10.1016/j.heliyon.2023.e23688.

References

[1] L. Bownass, S. Abbs, R. Armstrong, G. Baujat, G. Behzadi, R.D. Berentsen, et al., PAPSS2-related brachyolmia: clinical and radiological phenotype in 18 new cases, Am. J. Med. Genet. 179 (9) (2019) 1884–1894, https://doi.org/10.1002/ajmg.a.61282.

[2] M. Shohat, R. Lachman, H.E. Gruber, D.L. Rimoin, Brachyolmia: radiographic and genetic evidence of heterogeneity, Am. J. Med. Genet. 33 (2) (1989) 209–219, https://doi.org/10.1002/ajmg.1320330214.

[3] E. Flex, V. Imperatore, G. Carpentieri, A. Bruselles, A. Ciolfi, S. Pizzi, et al., A rare case of brachyolmia with amelogenesis imperfecta caused by a new pathogenic splicing variant in LTBP3, Genes (9) (2021) 12, https://doi.org/10.3390/genes12091406.

[4] D.C. Guo, E.S. Regalado, A. Pinard, J. Chen, K. Lee, C. Rigelsky, et al., LTBP3 pathogenic variants predispose individuals to thoracic aortic aneurysms and dissections, Am. J. Hum. Genet. 102 (4) (2018) 706–712, https://doi.org/10.1016/j.ajhg.2018.03.002.

[5] N. Intarak, T. Theerapanon, S. Thaweesapphithak, K. Suphapeetiporn, T. Porntaveetus, V. Shotelersuk, Genotype-phenotype correlation and expansion of orodental anomalies in LTBP3-related disorders, Mol. Genet. Genom. 294 (3) (2019) 773–787, https://doi.org/10.1007/s00438-019-01547-x.

[6] P. Kantaputra, Y. Guven, T. Kalayci, P.K. Özer, W. Panyarak, W. Intachai, et al., Expanding genotypic and phenotypic spectrums of LTBP3 variants in dental anomalies and short stature syndrome, Clin. Genet. 102 (1) (2022) 66–71, https://doi.org/10.1111/cge.14134.

[7] A. Noor, C. Windpassinger, I. Vitcu, M. Orlic, M.A. Rafiq, M. Khalid, et al., Oligodontia is caused by mutation in LTBP3, the gene encoding latent TGF-beta binding protein 3, Am. J. Hum. Genet. 84 (4) (2009) 519–523, https://doi.org/10.1016/j.ajhg.2009.03.007.

[8] S.L. Dugan, R.T. Temme, R.A. Olson, A. Mikhailov, R. Law, H. Mahmood, et al., New recessive truncating mutation in LTBP3 in a family with oligodontia, short stature, and mitral valve prolapse, Am. J. Med. Genet. 167 (6) (2015) 1396–1399, https://doi.org/10.1002/ajmg.a.37049.

[9] M. Huckert, C. Stoetzel, S. Morkmued, V. Laugel-Haushalter, V. Geoffroy, J. Muller, et al., Mutations in the latent TGF-beta binding protein 3 (LTBP3) gene cause brachyolmia with amelogenesis imperfecta, Hum. Mol. Genet. 24 (11) (2015) 3038–3049, https://doi.org/10.1093/hmg/ddv053.

[10] R. Kaur, I. Siddiqui, V. Mathur, M. Jana, M. Kabra, N. Gupta, Bi-allelic loss-of-function novel variants in LTBP3-related skeletal dysplasia: report of first patient from India, Am. J. Med. Genet. 182 (8) (2020) 1944–1946, https://doi.org/10.1002/ajmg.a.61629.

[11] B. Dabovic, Y. Chen, C. Colarossi, H. Obata, L. Zambuto, M.A. Perle, et al., Bone abnormalities in latent TGF-[beta] binding protein (Ltbp)-3-null mice indicate a role for Ltbp-3 in modulating TGF-[beta] bioavailability, J. Cell Biol. 156 (2) (2002) 227–232, https://doi.org/10.1083/jcb.200111080.

[12] I. Schrauwen, S. Helfmann, A. Inagaki, F. Predoehl, M.A. Tabatabaiefar, M.M. Picher, et al., A mutation in CABP2, expressed in cochlear hair cells, causes autosomal-recessive hearing impairment, Am. J. Hum. Genet. 91 (4) (2012) 636–645, https://doi.org/10.1016/j.ajhg.2012.08.018.

[13] G. Cui, A.C. Meyer, I. Calin-Jageman, J. Neef, F. Haeseleer, T. Moser, et al., Ca2+-binding proteins tune Ca2+-feedback to Cav1.3 channels in mouse auditory hair cells, J Physiol 585 (Pt 3) (2007) 791–803, https://doi.org/10.1113/jphysiol.2007.142307.

[14] T. Yang, N. Hu, T. Pangršič, S. Green, M. Hansen, A. Lee, Functions of CaBP1 and CaBP2 in the peripheral auditory system, Hear. Res. 364 (2018) 48–58, https://doi.org/10.1016/j.heares.2018.04.001.

[15] C. Kopanos, V. Tsiolkas, A. Kouris, C.E. Chapple, M. Albarca Aguilera, R. Meyer, et al., VarSome: the human genomic variant search engine, Bioinformatics 35 (11) (2019) 1978–1980, https://doi.org/10.1093/bioinformatics/bty897.

[16] S. Richards, N. Aziz, S. Bale, D. Bick, S. Das, J. Gastier-Foster, et al., Standards and guidelines for the interpretation of sequence variants: a joint consensus recommendation of the American College of medical genetics and Genomics and the association for molecular Pathology, Genet. Med. 17 (5) (2015) 405–424, https://doi.org/10.1038/gim.2015.30.

[17] H. Li, R. Durbin, Fast and accurate short read alignment with Burrows-Wheeler transform, Bioinformatics 25 (14) (2009) 1754–1760, https://doi.org/10.1093/bioinformatics/btp324.

[18] H. Li, B. Handsaker, A. Wysoker, T. Fennell, J. Ruan, N. Homer, et al., The sequence alignment/map format and SAMtools, J Bioinformatics 25 (16) (2009) 2078–2079.

[19] A. McKenna, M. Hanna, E. Banks, A. Sivachenko, K. Cibulskis, A. Kernytsky, et al., The Genome Analysis Toolkit: a MapReduce framework for analyzing next-generation DNA sequencing data, Genome Res. 20 (9) (2010) 1297–1303, https://doi.org/10.1101/gr.107524.110.

[20] G.H. Seo, T. Kim, I.H. Choi, Jy Park, J. Lee, S. Kim, et al., Diagnostic yield and clinical utility of whole exome sequencing using an automated variant prioritization system, EVIDENCE, Clin. Genet. 98 (6) (2020) 562–570, https://doi.org/10.1111/cge.13848.

[21] S. Köhler, M.H. Schulz, P. Krawitz, S. Bauer, S. Dölken, C.E. Ott, et al., Clinical diagnostics in human genetics with semantic similarity searches in ontologies, Am. J. Hum. Genet. 85 (4) (2009) 457–464, https://doi.org/10.1016/j.ajhg.2009.09.003.

[22] D. Greene, S. Richardson, E. Turro, Phenotype similarity Regression for Identifying the genetic determinants of rare diseases, Am. J. Hum. Genet. 98 (3) (2016) 490–499, https://doi.org/10.1016/j.ajhg.2016.01.008.

[23] J.T. den Dunnen, S.E. Antonarakis, Mutation nomenclature extensions and suggestions to describe complex mutations: a discussion, Hum. Mutat. 15 (1) (2000) 7–12, https://doi.org/10.1002/(sici)1098-1004(200001)15:1<7::Aid-humu4>3.0.Co;2-n.

[24] A.M. McInerney-Leo, C. Le Goff, P.J. Leo, T.J. Kenna, P. Keith, J.E. Harris, et al., Mutations in LTBP3 cause acromicric dysplasia and geleophysic dysplasia, J. Med. Genet. 53 (7) (2016) 457–464, https://doi.org/10.1136/jmedgenet-2015-103647.

[25] J.D. Fackenthal, L.A. Godley, Aberrant RNA splicing and its functional consequences in cancer cells, Dis Model Mech 1 (1) (2008) 37–42, https://doi.org/10.1242/dmm.000331.

[26] C.M. Sloan-Heggen, M. Babanejad, M. Beheshtian, A.C. Simpson, K.T. Booth, F. Ardalani, et al., Characterising the spectrum of autosomal recessive hereditary hearing loss in Iran, J. Med. Genet. 52 (12) (2015) 823–829, https://doi.org/10.1136/jmedgenet-2015-103389.

[27] M.M. Picher, A. Gehrt, S. Meese, A. Ivanovic, F. Predoehl, S. Jung, et al., Ca(2+)-binding protein 2 inhibits Ca(2+)-channel inactivation in mouse inner hair cells, Proc Natl Acad Sci U S A 114 (9) (2017) E1717–e1726, https://doi.org/10.1073/pnas.1617533114.

[28] B. Dabovic, Y. Chen, C. Colarossi, L. Zambuto, Obata Hjjoe, Bone defects in latent TGF-β binding protein (Ltbp)-3 null mice; a role for Ltbp in TGF-β presentation, J. Endocrinol. 175 (1) (2002) 129–141, https://doi.org/10.1677/joe.0.1750129.

[29] B. Dabovic, R. Levasseur, L. Zambuto, Y. Chen, G. Karsenty, D.J.B. Rifkin, Osteopetrosis-like phenotype in latent TGF-β binding protein 3 deficient mice, J Bone 37 (1) (2005) 25–31, https://doi.org/10.1016/j.bone.2005.02.021.

[30] M. Wu, G. Chen, Y.P. Li, TGF-β and BMP signaling in osteoblast, skeletal development, and bone formation, homeostasis and disease, Bone research 4 (2016), 16009, https://doi.org/10.1038/boneres.2016.9.

[31] S. Inamoto, C.S. Kwartler, A.L. Lafont, Y.Y. Liang, V.T. Fadulu, S. Duraisamy, et al., TGFBR2 mutations alter smooth muscle cell phenotype and predispose to thoracic aortic aneurysms and dissections, Cardiovasc. Res. 88 (3) (2010) 520–529, https://doi.org/10.1093/cvr/cvq230.

[32] M. Renard, B. Callewaert, F. Malfait, L. Campens, S. Sharif, M. del Campo, et al., Thoracic aortic-aneurysm and dissection in association with significant mitral valve disease caused by mutations in TGFB2, Int. J. Cardiol. 165 (3) (2013) 584–587, https://doi.org/10.1016/j.ijcard.2012.09.029.

[33] T. Burns, Y. Yang, E. Hiriart, A. Wessels, The dorsal mesenchymal protrusion and the pathogenesis of atrioventricular septal defects, Journal of cardiovascular development and disease (4) (2016) 3, https://doi.org/10.3390/jcdd3040029.

[34] K. Miyazono, A. Olofsson, P. Colosetti, C.H. Heldin, A role of the latent TGF-beta 1-binding protein in the assembly and secretion of TGF-beta 1, EMBO J. 10 (5) (1991) 1091–1101, https://doi.org/10.1002/j.1460-2075.1991.tb08049.x.

[35] S. Malik, Polydactyly: phenotypes, genetics and classification, Clin. Genet. 85 (3) (2014) 203–212, https://doi.org/10.1111/cge.12276.

[36] E.D. Austin, J.A. Phillips, J.D. Cogan, R. Hamid, C. Yu, K.C. Stanton, et al., Truncating and missense BMPR2 mutations differentially affect the severity of heritable pulmonary arterial hypertension, Respir. Res. 10 (1) (2009) 87, https://doi.org/10.1186/1465-9921-10-87.

[37] M. Speletas, A. Szilagyi, F. Psarros, D. Moldovan, M. Magerl, M. Kompoti, et al., Hereditary angioedema: molecular and clinical differences among European populations, J. Allergy Clin. Immunol. 135 (2) (2015) 570–573, https://doi.org/10.1016/j.jaci.2014.08.007.

[38] S.H. Bae, N.G. Robertson, H.J. Cho, C.C. Morton, D.J. Jung, J.I. Baek, et al., Identification of pathogenic mechanisms of COCH mutations, abolished cochlin secretion, and intracellular aggregate formation: genotype-phenotype correlations in DFNA9 deafness and vestibular disorder, Hum. Mutat. 35 (12) (2014) 1506–1513, https://doi.org/10.1002/humu.22701.

[39] D. Verdoodt, G. Van Camp, P. Ponsaerts, V. Van Rompaey, On the pathophysiology of DFNA9: effect of pathogenic variants in the COCH gene on inner ear functioning in human and transgenic mice, Hear. Res. 401 (2021), 108162, https://doi.org/10.1016/j.heares.2020.108162.

[40] R. Kingdom, C.F. Wright, Incomplete penetrance and variable expressivity: from clinical studies to population cohorts, Front. Genet. 13 (2022), 920390, https://doi.org/10.3389/fgene.2022.920390.